02,13

Structure, Morphology, Transport, and Mechanism of Oxygen Loss in YBa$_2$Cu$_3$O$_{7-delta}$ Thin Films Obtained by Pulsed Laser Deposition with Velocity Filtration in Erosion Plume

© *A.I. Il'in* [1], *A.A. Ivanov* [2], *V.K. Egorov* [1]

[1] Institute of Microelectronics Technology and High Purity Materials, Russian Academy of Sciences,
Chernogolovka, Russia
[2] National Research Nuclear University „MEPhI",
Moscow, Russia

E-mail: alivil2017@yandex.ru

We report the study of YBa$_2$Cu$_3$O$_{7-\delta}$ films, synthesized on SrTiO$_3$(100) substrates by pulsed laser deposition with velocity filtration, using X-ray diffractometry, transport measurements, and scanning electron microscopy. We have revealed the dependence of the structure of $100-200$ nm thick YBa$_2$Cu$_3$O$_{7-\delta}$ films on deposition time and velocity of particles in erosion plume, set by velocity filter. After deposition, the films, or their part, close to the substrate, consisted of $3-10$-nm crystals with oxygen index $\delta = 0.08$, the same as in the target. For deposition time from 10 to 60 min, we observed the growth of regular pyramids with triangular and quadrangular bases from 20 to 500 nm in size at the base and spiral pyramids with polygonal bases on the film surface. The maximum oxygen loss up to $\delta = 0.35$ and $T(R = 0)$ up to 77.4 K coincided with the appearance of spiral pyramids up to 100 nm-high. These findings evidence in favor of oxygen depletion of the top layers of YBa$_2$Cu$_3$O$_{7-\delta}$ thin films through the formation and growth of oxygen-deficient pyramids on their surface. The oxygen index in the range of $\delta = 0.08-0.15$ in both nanocrystals and regular pyramids of $20-300$ nm in size provided $T(R = 0) = 84-87$ K and the width of superconducting transition $\Delta T = 2.5-3.5$ K.

Keywords: pulsed laser deposition, surface morphology, film transport properties, film evolution, SrTiO$_3$.

1. Introduction

YBa$_2$Cu$_3$O$_{7-\delta}$ (YBCO) thin films, regardless of the deposition method, have a relief on the surface, often in the form of pyramids, which is revealed by atomic force microscopy and SEM [1–4] methods. The appearance of relief (the minimum value of which in epitaxial films cannot be less than 1.1 nm — period of the lattice along the crystallographic axis C), inextricably connected with the atomic structure, degrades the functionality of films and 2D devices based on them. In this regard, understanding the mechanisms of the formation of atomic surface structure in the most demanded in terms of its electrophysical characteristics oxygen-deficit films YBCO with $0 \le \delta \le 0.4$ and also the features of crystallization is an important and practical knowledge that improves the technology of pulsed laser deposition (PLD) of films [5,6]. The identification of the causes of changes in surface morphology and oxygen distribution in films is also necessary for optimizing the production of nanostructures based on high-temperature superconductors (HTSC).

Optimally doped oxygen-deficiency thin films with an index of $y = 7 - \delta \approx 6.85$ and equilibrium structure have an end temperature of superconducting transition (SP) $T(R = 0) = 85-90$ K. The oxygen doping index of YBCO thin films is calculated from the X-ray spectrum by its connection lattice parameter c and from the dependence $R(T)$ $T(R = 0)$ [7–10] are determined. Doping can also be estimated at the initial temperature deviation from the linear temperature dependency of $R(T)$ oxygen-deficiency thin films, which we designate hereafter as T_{dev} [8–10]. The surface relief of the films depends on the oxygen pressure in the deposition chamber during the deposition of the film and the distance between the substrate and the target — with an increase in pressure or decrease in the distance between the substrate and the target mainly two-dimensional growth mode were observed, otherwise, a — growth regime with pyramid formation, including spirals. At pyramid spiral growth, the surface roughness of the films reached about 82 nm. The different growth method was explained by changes in the surface diffusion rate by 2 order of magnitude [4] occurring during deposition under different conditions. Of all the elements constituting YBCO, structural oxygen is known to be the most mobile, and its concentration depends on both deposition conditions and annealing conditions. Annealing in neutral atmospheres leads to the loss of oxygen; moreover, it can escape even when annealed in the oxygen atmosphere. In work by Reiner *et al.* [11] the initial oxygen diffusion temperature was found to be slightly above 240°C, the nature and diffusion mechanism

Deposition, filtration, structure characteristics and SP-transition of films

Film №	d, mm	V_O, 10^4 m/s	N, Hz	Z, Å/s	T, K $(0.9R_{92})$	ΔT, K $(0.1R_{92})$	ΔT, K K	$T(R=0)$, K	ρ_{300}, $\mu\Omega\cdot$cm	δ^*	FWHM (005), deg**
1	10	2.0	28	4.9	89.2	86.4	2.8	85	2300	0.12 (0.1)	(0.9)
2	10	2.3	33	5.8	90.5	88	2.5	85.8	2300	0.09 (0.15)	0.11
3	10	1.5	21	6.2	90	86.6	3.4	84	1400	0.17 (0.22)	0.211
4	8	1.9	21	6.1	90.2	87.6	2.6	84	1400	0.07 (0.22)	0.14 (0.7)
5	6	2.1	4.5	0.5	82	< 77.4	–	< 77.4	1000	0.24 (0.35)	(0.58)
6	6	3.0	6.5	1.1	84	80.5	3.5	77.4	1000	0.35 (0.35)	0.115
7	–	–	15	4.5	90.8	88.4	2.4	87	1200	0.08 (0.15)	0.15 (0.58)

N o t e. * The numbers without brackets show the result of determining δ by c-parameter, and in brackets — by T_{dev} derived from relation $R(T)$ [8–10].
** The result of determination of FWHM at an angular dependence of intensity (005) in the focusing geometry of Bregg−Brentano $\theta-2\theta$, and in brackets — from the rocking curves [19], representing an angular dependence of intensity (005) is shown.

were not established. For the YBCO film produced by laser deposition followed by annealing in oxygen 400 mbar at a temperature of 400°C, the oxygen index of $y = 7-\delta$ decreased with the growth of δ from 0 on the free surface to 0.4 at the boundary of the film−substrate [11]. After a vacuum exposure, the value of δ varied from 1.05 on the free surface to 0.25 at the substrate.

The use of high-speed erosion plume filtration for PLD resulted in the production of YBa$_2$Cu$_3$O$_{7-\delta}$ superconducting films with a thickness of $100-200$ nm as a surface consisting of pyramids with steps on the lateral slopes of $1-2$ nm, base diameter up to $1.5\,\mu$m, height up to 40 nm (inclination 2.5%), and spiral and regular pyramids with triangular and polygonal bases [10,12]. Films with better characteristics and morphology can be used to create structures with a lateral resolution of ~ 100 nm and $T\,(R = 0)$ to 86 K for basic research and application problems [13–17]. In this work, the results of X-ray diffraction analysis, morphological and transport changes of the film properties were brought into line with the oxygen index. The evidence suggests a mechanism for oxygen loss by the top layer of thin YBCO films through the formation and growth of oxygen-depleted pyramids. We also made an assumption about oxygen diffusion by defects in the spiral pyramids along their heights. This effect was observed on films grown during the deposition of $50-60$ min with high-speed laser plume filtration.

2. Procedure

The films were deposited on monocrystalline plates SrTiO$_3$(100), the surface of which had a roughness scale of up to 2 nm and a mean squared roughness deviation of $Rq = 0.14$ nm. Plates measuring 5×10 mm and 0.5 mm thick before depositon were cleaned in a mixture (H$_2$SO$_4$ + HNO$_3$) and washed in distilled water. Films

$150-200$ nm thick were precipitated with high-speed erosion plume filtration to produce $T(R = 0) = 85-85.8$, 84, 77.4 K while 300 nm — without filtration (table). The PLD unit, detailed in [10,12], consisted of excimer laser CL7100 (wavelength 248 nm, pulse length 15 ns), upgraded vacuum setup VUP-4, equipped with a Varian pump SH-110, and Varian TPS-compact turbomolecular pumping system. The frequency of pulses of ablated material to the substrate (filtering frequency N) was set by the laser launch synchronization system with the position of holes in the disk and in our experiments was equal to the frequency of laser pulses. The limiting frequency of laser pulses at deposition was less than the disk speed (n), which varied from 90 to 160 Hz, so the frequency divider was used at the launch of the laser, so the ratio of n/N in various experiments was 5 to 20. The minimum velocity of the particles passing through the hole in the disc, hereinafter called cut-off rate, is $V_0 = L/T$, where the disk distance from the target is $L = 30-35$ mm, and $T = d/(2\pi Dn)$; where D — distance from the hole to the axis (75 mm), the diameter of this hole is d. The thickness of the films was determined using a stylus profiler Dektak-150. The deposition rate Z was calculated by dividing the film thickness by the deposition time. Surface morphology was studied in SAM EVO-50. $R(T)$ films were measured on chips sized 5×10 mm by a four-probe method. Contacts in the form of four strips of silver with a width of 0.5 mm were deposited on the YBCO film across the long side of the chip with a distance between the inner potential stripes of 7 mm. On the dependence of $R(T)$ for each sample, the following values were determined: T_{dev} — the temperature of the beginning of the deviation $R(T)$ from the straight line in the part of the temperature interval before SP transition; R_{92} — the resistance in normal state before the SP transition, $T(R = 0.9R_{92})$, $T(R = 0.1R_{92})$ — transition temperatures at 0.9 and 0.1 of R_{92}, respectively, $\Delta T = T(R = 0.9R_{92}) - T(R = 0.1R_{92})$, $T(R = 0)$ — transition termination temperature.

An X-ray diffraction study (XRD) was carried out using a HZG-4 diffractometer with a fixed anode and a BSV-28 tube (CuK_α $\lambda = 1.54178$) at 25 kV and current 20 mA in the focusing Breg−Brentano $\theta−2\theta$ [18] geometry with radius $r = 235$ mm. The initial radiation flux was formed by a vertical slit 0.1 width and a height of 10 mm, and also by a horizontal Soller slit with a distance between the plates 1 mm. With X-ray source focal width 1.0 mm, sampling angle 6° and distance from focal spot to cropping slit 50 mm, a ray flux with horizontal divergence $\Delta\varphi = 0.2°$ was formed. The vertical flow rate determined by the application of the Soller slit was 2°. However, the use of the Soller slit in front of the detector slit made it possible to reduce the angular divergence in the recorded reflections to $\Delta\psi = 0.2°$. The diffraction lines were recorded by a scintillation detector with a gap-cutting width of 0.1 mm and a height of 10 mm. The diffraction data was collected both in the analog mode and in the step-by-step scanning mode with the recording step interval of each dimension from 0.01 to 0.005° for 10 s. The application of a filter of Ni-film 20 μm thick reduced the intensity of CuK_β lines by 500 times while reducing the intensity of CuK_α lines by only half. Energy discrimination of the registered diffraction lines was performed with a single-channel analyzer of the SCA-550 type by „Ortec". When it was used, the contribution of the „white" component to the intensity of the registered diffraction lines did not exceed 5%. The oxygen content of the films was calculated from precision measurements of the angular position of the maximum reflection (005). The misorientation of the monocrystalline film blocks was determined from the so-called rocking [19] curves representing the angular dependence of the intensity in the reflection region (005) of YBCO ($2\theta_{005} \approx 38.1°$) with the counter stationary at the position of maximum intensity by their FWHM.

3. Results

Films 300, 150−200 nm thick, deposited without filtration and with laser erosion plume filtering, respectively (table), had characteristic oxygen deficiency of $R(T)$ [10]. Films 7 obtained without filtration were with low $\rho_{300} = 1200\,\mu\Omega \cdot cm$ and high $T(R = 0) = 87$ K (table). Films 1−2, 3−4, 5−6 had a value of $T(R = 0) = 85−85.8$, 84, 77.4 K and resistances $(\rho_{300}) \sim 2300$, ~ 1400, $\sim 1000\,\mu\Omega \cdot cm$, respectively, i.e., the less ρ_{300}, the less $T(R = 0)$ was. Film 7 obtained without filtration is out of this row. With the same high $T(R = 0)$ as the samples 1 and 2, and close oxygen deficiency values δ, it is two times less as the specific resistance ρ_{300}, 1200 and 2300 $\mu\Omega \cdot cm$, respectively. This may be due to the different transparency of the inter-grained boundary, as indicated by the difference in FWHM of the peak curve (005) of these samples.

On plume substrate diffraction patterns collected in analog mode, only peaks of coherent scattering regions (CSR) ($h00$) of the substrate and ($00l$) of YBCO were observed,
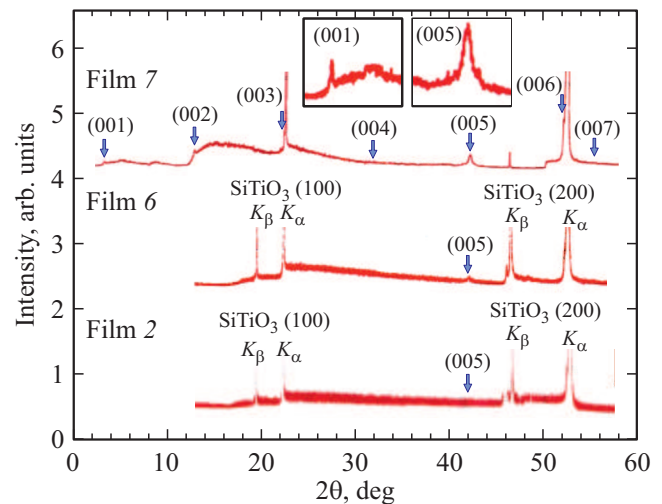

Figure 1. Diffraction patterns $\theta−2\theta$ of YBa$_2$Cu$_3$O$_{7−\delta}$ films on SrTiO$_3$ (100) substrates: film (film) 7 — close-up peaks (001) and (005) are shown in the insets, which intensity ratio was used to determine oxygen deficiency $\delta = 0.08$ (diffraction pattern was taken with the Ni-filter) [7]; films 6, 2 even when taken without the Ni-filter are missing some of the diffraction maxima.

depending on deposition conditions (Fig. 1). The lattice parameter of YBCO ($00l$), calculated from the angular position of the peaks, varied from 1.168 to 1.173 nm (table), corresponding to oxygen-deficient films. The diffraction pattern of film 7, obtained without filtering the erosion plume, except for the Bragg peaks ($00l$), contained diffuse halos, the most significant in intensity at $2\theta = 12−30$, $50−60$ degrees (Fig. 1). Peak intensities (001) and (002) were the same and half as much as (005), while peaks (004) and (007) were slightly above the background. Reflection maximums (003) and (006) of the YBCO coincided with strong reflections (001) and (002) of SrTiO$_3$ substrate at $2\theta = 22.777$ and 46.523° respectively. Therefore, the reflection (005) at $2\theta = 38.609°$, which did not coincide with the diffraction angles from the halo and substrate, was in the preferred position for the study. Estimates of oxygen deficiency in film 7, made both in relation to the reflectivity (001)/(005) [7], and c-period of the lattice, gave a value of $\delta = 0.08$, and corresponded to the oxygen concentration in the target. In films 6 and 2 there were two diffusion halos at $2\theta = 12−46$ and 48−58° and reflexes (003), (005), (006) in film 6 and (006) in film 2 (Fig. 1).

Intensity of reflex (005) in film 7 obtained without the filtering of the plume was $\sim 170\,000$, and reduced to a thickness of 175 nm is $(170\,000/300) \cdot 175 = 99\,167$, which equals an intensity of 100 000 from film 6. The FWHM size in film 7 (0.15) is 0.03° larger than that in film 6 (0.12), consistent with the notions of the same stress relaxation in [7] films, and the oxygen deficit δ was 0.08 and 0.35, respectively. Thus, at the same CSR intensities, close to the FWHM values (difference of 20%) in film 6 the value of δ was greater by 4.5 times, which was the reason for
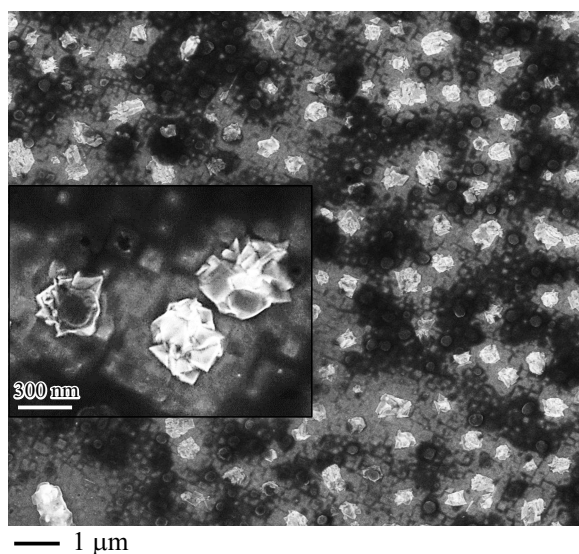
Figure 2. Surface of film *5* with high spiral pyramids with polygonal bases up to 80 nm in SEM. The inset depicts the spiral pyramids above the rectangular pyramids.

the decrease of $T(R = 0)$ to 77.4 K. The surface structure of film *6* is represented by both rectangular base pyramids and spiral pyramids (Fig. 2) up to 100 nm, which were not present in other films. Thus, the oxygen deficiency δ is caused by longer deposition time and correlates with the appearance of large spiral pyramids on the surface.

The δ values calculated from the angular position of the peak maximum (005) (Fig. 3) were 0.08 for film *3* and 0.17 for film *4*, which should correspond to $T(R = 0) = 87$ K in film *3* (as in film *7*) and 84 K in film *4*. However, both films at FWHM $= 0.2°$, peak height 17 500 and FWHM $= 0.14°$,

peak height 7500, respectively, had $T(R = 0) = 84$ K. Deposition of film *4* at a higher rate of particle velocity than deposition of film *3* formed a 2 times less intense peak from CSR, but stronger oxygenated. The lower CSR intensity meant that a larger proportion of the nanocrystals formed diffuse halo. The nanostructure reduces the temperature interval of the transition SP in sample *4* (table), probably maintaining a high gradient of oxygen concentration along the film thickness. In this case it can be assumed that it has a lower oxygen diffusion coefficient, and hence a high ρ_{300}. Within the angular peak interval (005) a weaker maximum was found at $2\theta = 38.38°$ in film *3* and $2\theta = 38.52°$ in film *4* (Fig. 3, inset *A*). If we assume that additional maxima (005) are due to different oxygen doping, then their content in the CSRs generating them will be higher than in the main peak, and δ will be ~ 0.08 and 0 in *4* and *3* films, respectively, and the HTS phase diagram of these films δ will be on different sides of the maximum of the inverted parabola, and this determines the equal $T(R = 0) = 84$ K. Peak intensity (005) ~ 1500 with $\delta = 0.09$ in film *2* assumes a share of $\sim 1-2\%$ of the amount of CSR in film *7* with a peak height of 150 000 with almost $T(R = 0) = 85.8$ and 87 K, respectively. Thus, the film *2* consists mainly of nanocrystals (which may have its own features [20]), and films *3, 4, 6* — from the multi-doped Bragg CSR pyramids.

Intensity of diffraction peak on peak curve (005) for film *7*, normalized by thickness 175 nm $(120\,000/300 \cdot 175) = 70\,000$ less than the diffraction intensity of film *5*, which equals 90 000, i.e., the structure of film structure *5* is less relaxed as annealing reduces the height [7]. The number of additional maximums on rocking curves characterizing the preferential angle deviations of monocrystalline film blocks from [00*l*], decreases with the
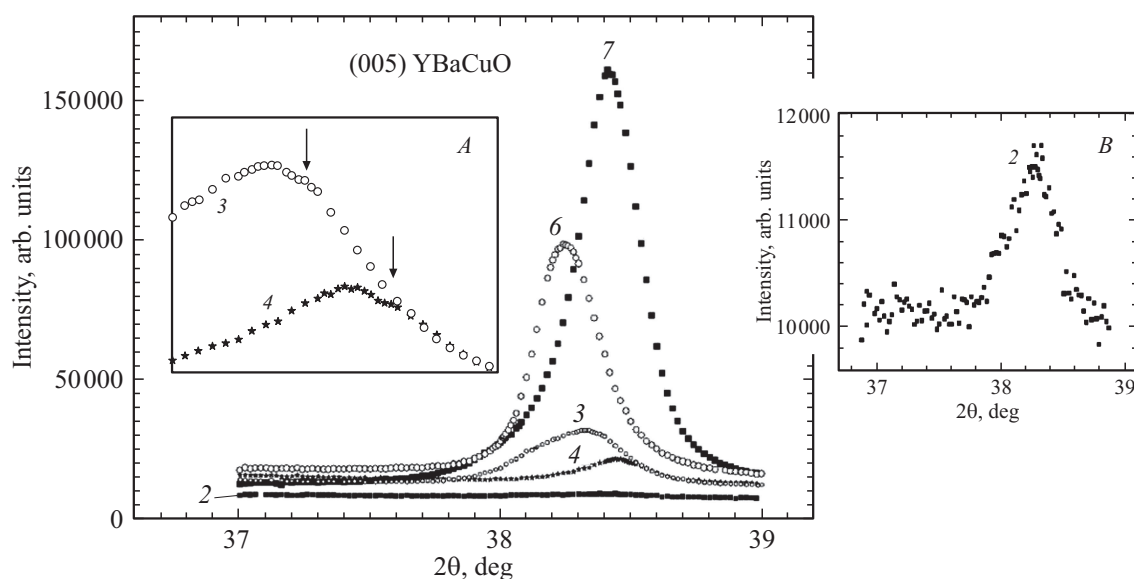

Figure 3. Diffraction peaks (005) of YBaCu$_3$O$_{7-\delta}$ films with different $T(R = 0)$: *2* — 85.8, *3* and *4* — 84, *6* — 77.4, *7* — 87 K. Close-ups and arrows in inset *A* show additional diffraction peaks of *3* and *4* films, and on *B* – the height of the diffraction peak of *2* film.
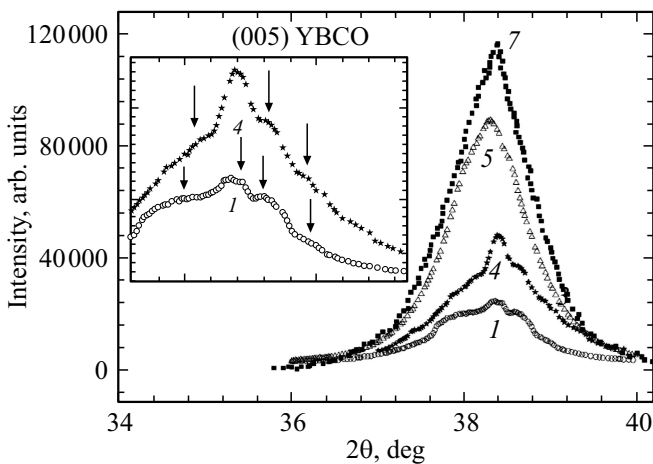
Figure 4. Peak rocking curves (005) films $YBa_2Cu_3O_{7-\delta}$, with different $T(R=0)$: *1* — 85.8, *4* — 84, *5* — 77.4, *7* — 87 K. In the inset, close-ups of the rocking curves show the approximate angles of the additional diffraction intensities in the angular range of the rocking of samples *1* and *4*.

increase of peak height from 4 in film *1* to 2 in film *5*, while semblance of the shape of the curves with the increase of the height of the main peaks in films *1* and *4* (Fig. 4) is kept. The angular position of the additional maxima in films *1* and *4* is approximately maintained, indicating both the regularity of their angular position formation and the regularity of the displacement of the main maxima towards smaller angles. FWHM in films *7, 5, 4, 1* were 0.58, 0.58, 0.7, 0.9 deg (table), respectively, i.e., film *1*, with the lowest intensity of diffraction peak (005) $\sim 26\,000$, has the most disoriented monocrystalline blocks at the lowest deposition time. The decrease in FWHM with the increased deposition time indicates a decrease in the disorientation of monocrystalline blocks in films at high deposition times. More oriented (with smaller FWHM) films *5* and *7* were in one case formed by long-term deposition, and in other — by deposition without filter, i.e., from the flux, in which along with the finely dispersed part there were large particles. However, when growing in the filtration mode, epitaxy conditions were closer to optimal.

4. Discussion

The presence in the range of the angular width of main peak (005) (Fig. 3) of an additional CSR maximum indicates an inhomogeneous distribution of the chemical composition of the crystal lattice, probably oxygen as the most mobile element [11] in films *3* and *4*. If the heights of the central diffraction intensity maxima characterize the fraction of particles forming them, then the formation of the Bragg CSRs after deposition with filtration was least in film *1* and *2*, and maximum — in films *5* and *6*, reaching relations of values ~ 70 times. The most significant

diffuse halos observed for film *7* in the corner intervals of $2\theta = 12-30$, $50-60$ deg they Selyakov−Sherrer formula:

$$D = n\lambda/\beta\cos(\theta),$$

where D — the size of the CSR, n — the reflection order, β — line widening in radians, θ — the scattering angle, give an estimate of the size of nanocrystals in ~ 4 and $\sim 8-10$ nm, respectively. Similar calculation for two diffusion halos at $2\theta = 12-46$ and $48-58$ deg (Fig. 1) in films *6* and *2* gives values of $\sim 2-3$ and $\sim 8-10$ nm. Since the cut pyramids on the surface of the films *1* and *2* are rare and do not form a solid cover [10], it is the nanosized crystals that have measured SP characteristics (table) with $T(R=0) = 85-85.8$ K. Thus, nanoscale crystals predominate in films *1* and *2* and in films *5, 6, 7* — crystals over 200 nm (size outside the applicability of the Selyakov−Sherrer formula), which almost does not affect $T(R=0)$. In films *6* and *7* oxygen loss δ was 0.35 and 0.08, and $T(R=0)$ was 77.4 and 87 K, respectively, at close FWHM values, meaning $T(R=0)$ is the oxygen deficit. Nanocrystals predominate in films *1* and *2* which seem to hold oxygen, giving films *1* and *2* the best characteristics of SP with $\Delta T = 2.5-2.8$ K, while films *3* and *4* consist of a mixture of nanocrystals and multi-doped cut pyramids. It can be assumed that the nanocrystalline structure compared to the structure giving the Bragg reflections, even with an optimal amount of oxygen, good $T(R=0)$ and SP characteristics forms high ρ_{300}, probably due to the increase in the volume of films and/or a decrease in the transparency of the intercrystalline interfaces.

The numbers of additional intensity peaks *4, 3, 2* on film rocking curves *1, 4* and *5*, respectively, indicate different angles of individual monocrystalline film blocks relative to orientation [005] depending on the deposition conditions (Fig. 2), and their formation happens simultaneously. Some similarity in the shape of the curves and the proximity of the angular positions of part of the additional maxima in films *1* and *4* indicate the non-random nature of the orientations. The peak amplitude increases as the number of additional maxima decreases. Typically, such processes occur when a structure is recrystallized to form a stronger texture, as in this case. As previously established [6], pyramids on the surface of films consist of rods up to 10 nm thick. The rods are likely to grow from the same size of nanocrystals that give diffuse halos, and the pyramids composed of them are not formed directly from the products of the erosion plume, but grow on favorably oriented volumes of deposited material. Such growth is facilitated by the finely dispersed component of the plume, which disperses at high speeds (small clusters, atoms and ions from target), which facilitates the migration of already adsorbed atoms. The predominant growth of individual crystals was previously observed [21] on transverse slices in aluminium films. The formation of coherent boundaries [22,23] between individual rods during long deposition time forms a good texture. The higher FWHM value of the film rocking curve *1* than in the

film *5* and the lower height of the central maximum can be considered as an argument for the proposed nature of the texture (Fig. 3). The lateral maxima on the rocking curve in film *7*, precipitated mainly by particles up to 1000 nm [12] may not appear due to the small amount of finely dispersed component of the erosion plume.

Almost all oxygen deficiency values δ (table), calculated from the YBCO (005) lattice parameter measurements, were less than those obtained using the $R(T)$ [7–10] — probably due to both a less orderly and uneven distribution of cations and oxygen and a more defective crystal structure [7,24]. Close oxygen deficiency values δ are obtained in these methods at low deposition rates, i.e., in films with relaxed structure. Oxygen distribution heterogeneity in films *3* and *4* appears on the diffractograms $\theta-2\theta$ as two diffraction peaks (005) (Fig. 3). The additional diffraction maxima correspond to a higher oxygen uptake than the main one, while the approximate values of δ, calculated by their angle position for films *3* and *4*, are 0.08 and 0.0, respectively. Since additional diffraction maxima with less oxygen deficiency δ are observed in films with low deposition rate, and the number of pyramids in them and their size is larger, the main maximum forms diffraction from large pyramids. Thus, the films with oxygen disorder consist of pyramidal crystals of the upper layer with different oxygen doping and the lower layer, which is heavily doped. The difference in the doping of the upper and lower layers of oxygen of $\Delta\delta = 0.1$ coincides with the results of the annihilation positron spectroscopy with the alternating energy positron beam in 230 nm [11], films produced after vacuum annealing. The transport characteristics of these films will be determined by all crystals simultaneously. Therefore, the films *4* with two Bragg CSR maxima, among which there are with $\delta = 0.08$ (as in film *7*), have a high $T(R = 0.9R_{92})$, which determines the best performance of the superconducting phase.

It is generally accepted that the growth of YBCO films is most consistent with the Volmer−Weber mechanism, where atoms and small clusters bind more closely than the substrate to three-dimensional islets, then grow into textured film. With PLD precipitation with a high-speed filtration of ~ 30 Hz in films *1* and *2* Bragg reflections have little or no intensity (Fig. 1) and widespread diffuse halos indicate a predominance of a $2-10$ nm nanocrystalline structure. The flux od ablated material does not have time to repeat the crystal structure of the substrate, and during the time between the impulses $\sim 3 \cdot 10^{-2}$ s on the surface only individual pyramids with triangular bases of $\sim 20-100$ nm grow [10,12]. With cutting, they give a low-intensity Bragg diffraction, and therefore it is impossible to determine a good epitaxy by using X-ray analysis in these films. With an increase in deposition time, a surface is formed from the rectangular base pyramids, which correspond in films *3* and *4* to a segregation into areas enriched and depleted with oxygen. The oxygen-rich and oxygen-poor regions belong to the pyramids that give the Bragg diffraction. The oxygen-enriched areas vanish and the oxygen content drops

in slowly deposited films *5* and *6*, obtainde at low deposition rate. In these films among the pyramids with rectangular bases appear higher pyramids from the multifaceted base (Fig. 2, inset). Since they appear on the background of rectangular base pyramids in films with greater deposition time and have higher altitude, they grow faster, probably with the participation of diffusion of atoms, including oxygen, on the defect of the pyramid along its height to the top (Fig. 4). The increase in the size of the pyramids is accompanied by the loss of oxygen from the film layers attached to the substrate. It is possible that this is facilitated by the reduction of vacancies and other defects in large oriented pyramid crystals. Given the large number of screw pyramids and their relative regularity, it can be assumed that the growth of deposition films is not due to the Volmer−Weber mechanism, but to the Stransky−Krastanov mechanism, where in a solid layer of sediment covering the substrate, structural defects are formed in the form of dislocations on which the embryos of the upper layer grow, forming an epitaxial film. The mechanism of oxygen loss found is likely to occur without the formation of nanocrystals, if the embryos have time to grow on the substrate into pyramids with dimensions giving the Bragg reflections. In any case, the loss of oxygen will be due to the growth of pyramids first with rectangular bases and then spiral pyramids.

5. Conclusion

When pulsed laser deposition of films with high-speed filtering erosion plume frequency of $4-33$ Hz film layer adjacent to the substrate is enriched with oxygen, its content corresponds to $\delta = 0.08$, and oxygen-depleted layers are on the free surface. The oxygen enriched layer consists of nanoscale crystals and is detected on diffractograms on diffuse halo. The oxygen-depleted layer consists of pyramid-cut crystals on the surface of the film, which is detected in the SEM and on the diffraction patterns of the Bragg diffraction. With the emergence of crystalline pyramids on the surface, oxygen deficiency increases, as measured by the c-grid parameter and film transport characteristics. Oxygen losses with the degradation of HTS properties are particularly rapid when spiral pyramid films are formed in the structure. The established facts suggest a mechanism for depletion the upper layers of thin films $YBa_2Cu_3O_{7-\delta}$ by oxygen through the formation and growth of oxygen-deficiency pyramids on their surface as some new phase.

Crystal defects and structural disordering formed during deposition can be a significant factor in altering the lattice parameters of thin films produced by PLD with high-speed erosion plume filtration. Therefore, the c-lattice parameter is not an unambiguous oxygen content function, the definition of which in such thin films in this way becomes incorrect. Despite possible structural disordering and high ρ_{300}, filtered films have good characteristics: $T(R = 0) = 87-84$ K and width of SP $\Delta T = 2.8-2.5$ K.

The SP and $T(R = 0)$ characteristics of films depend on the layer with optimal oxygen doping. In this case, the $R(T)$ largely reflects the transport properties of the optimally doped layer, as opposed to X-ray diffraction analysis, which produces results averaged by film volume.

Funding

Conflict of interest

The authors declare that they have no conflict of interest.

References

[1] B. Dam, J. Rector, M.F. Chang, S. Kars, D.G. de Groot, R. Griessen. Appl. Phys. Lett. **65**, *12*, 1581 (1994).

[2] Pulsed Laser Deposition of Thin Films / Eds D.B. Chrisey G.K. Hubler. John Wiley & Sons Inc. N.Y. (1994).

[3] C. Gerger, D. Anslemetti, J.G. Bednorz, J. Mannhart, D.G. Schlom. Nature **350**, 279 (1991). https://doi.org/10.1038/350279a0

[4] B. Dam, J.H. Rector, J.M. Huijbregtse, R. Griessen. Physica C **305**, *1–2*, 1 (1998).

[5] R. Arpaia, D. Golubev, R. Baghdadi, R. Ciancio, G. Drazic, P. Orgiani, D. Montemurro, T. Bauch, F. Lombardi. Phys. Rev. B **96**, *6*, 064525 (2017).

[6] A.I. Il'in, A.A. Ivanov, O.V. Trofimov, A.A. Firsov, A.V. Nikulov, A.V. Zotov. Russ. Microelectron. **48**, *2*, 119 (2019).

[7] J. Ye, K. Nakamura. Phys. Rev. B **48**, *10*, 7554 (1993).

[8] N.E. Hussey. J. Phys.: Condens. Matter **20**, *12*, 123201 (2008).

[9] T. Ito, K. Takenaka, S. Uchida, Phys. Rev. Lett. **70**, *25*, 3995 (1993).

[10] A.I. Il'in, A.A. Ivanov. FTT **63**, *9*, 1209 (2021) (in Russian).

[11] M. Reiner, T. Gigl, R. Jany, G. Hammerl, C. Hugenschmidt. Phys. Rev. B **97**, *14*, 144503 (2018).

[12] A.I. Il'in, O.V. Trofimov, A.A. Ivanov. FTT **62**, *9*, 1555 (2020) (in Russian).

[13] V.L. Gurtovoi, A.I. Ilin, A.V. Nikulov. Phys. Lett. A **384**, *26*, 126669 (2020).

[14] A.A. Burlakov, V.L. Gurtovoy, A.I. Il'in, A.V. Nikulov, V.A. Tulin. Pis'ma v ZhETF **99**, *3*, 190 (2014) (in Russian).

[15] A.A. Burlakov, A.V. Chernykh, V.L. Gurtovoi, A.I. Il'in, G.M. Mikhailov, A.V. Nikulov, V.A. Tulin. Phys. Lett. A **381**, *30*, 2432 (2017).

[16] V.L. Gurtovoi, A.I. Il'in, A.V. Nikulov, V.A. Tulin. Low Temper. Phys. **36**, *10*, 974 (2010).

[17] R. Arpaia, D. Golubev, R. Baghdadi, R. Ciancio, G. Drazic, P. Orgiani, D. Montemurro, T. Bauch, F. Lombardi. Phys. Rev. B **96**, *6*, 064525 (2017).

[18] H.P. Klug, L.E. Alexander. X-Ray diffraction procedures. John Wiley & Sons, N.Y. (1974). 966 p.

[19] L.V. Azarov. X-Ray Diffraction. McGraw-Hill Book Company, N.Y. (1974). 664 p.

[20] A.I. Il'in, V.S. Kraposhin. Poverkhnost'. Fisika, khimiya, mekhanika *6*, 5 (1985) (in Russian).

[21] A.I. Il'in, E.E. Glikman, I.Yu. Borisenko, N.D. Zakharov, V.V. Starkov. Poverkhnost'. Fisika, khimiya, mekhanika **94**, 77 (1991) (in Russian).

[22] A.I. Il'in, A.V. Andreeva, B.N. Tolkunov. Mater. Sci. Forum. **207–209**, 625 (1996).

[23] A.I. Il'in, A.V. Andreeva. Fizika metallov i metallovedenie, **80**, *2*, 132 (1995) (in Russian).

[24] C.B. Eom, J.Z. Sun, B.M. Lairson, S.K. Streiffer, A.F. Marshall, K. Yamamoto, S.M. Anlage, J.C. Bravman, T.H. Geballe, S.S. Laderman, R.C. Taber, R.D. Jacowitz. Physica C **171**, *3–4*, 354 (1990).